

Parameter identification for a hyperelastic material model of an elastomer rubber boot

In order to develop a stable and reliable hyperelastic material model for a rubber boot of a constant velocity (CV) joint, optiSLang was used for parameter identification and direct optimization to fit the simulated stress strain curves to the experimental data.

Introduction

IFA develops and manufactures side and longitudinal drive shafts as well as their corresponding components, such as cross and constant velocity joints. Depending on the field of application, there are different CV joints.

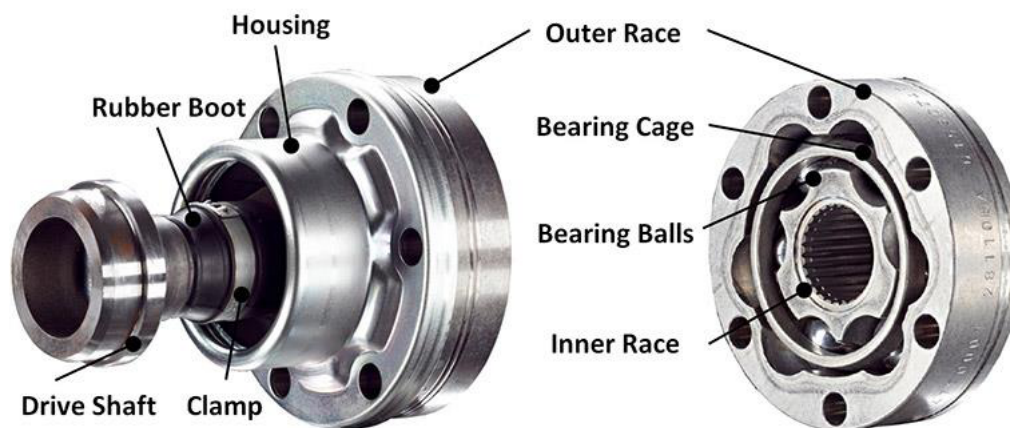


Fig.: 1: CV joint manufactured by IFA

The purpose of these joints is to transmit torque, to bend the shaft and to ensure a length compensation due to the kinematics of the drive train. The advantage of them is that the rotary movement can be uniformly transmitted at all angular positions. CV joints essentially consist of the following steel components: hub, outer ring, bearing cage with balls, the sealing cap as well as the connecting part pin and the sealing component elastomer rubber boot (Fig. 1). The rubber boot is clipped on the pin as well as in the crimp of the sealing cap where it flexibly seals the CV joint. This prevents a contamination from the outside even in bended position or during length compensation. Furthermore, the lubrication of the joint will be ensured. In the case of a positive length compensation, the rubber boot will be exclusively stretched. During a negative length compensation of the joint, the rubber boot rolls off without creasing on the inside of the sealing cap as well as on the pin and the hub. The reduction of the working space simultaneously leads to a pressure increase inside the joint. This may cause an "s-punch shape" deformation of the rubber boot (Fig. 2). The resulting contact with other components could damage the surface of the boot, eventually leading to its failure and causing even more damage to other joint components. The aim of the simulation is to

obtain a reliable prognosis of the deformation of the rubber boot as well as to conduct a leakage test for predefined joint positions.



Fig. 2: "S-punch shaped" deformation (left) and optimal rolling off behavior (right) of the rubber boot

Methodical approach

For the generation of a hyperelastic material model, measurement data from two material tests were used and the corresponding material parameters were determined by curve fitting.

Measurement data and material model

For the curve fitting, tensile as well as shear test data (simple shear tests) were available in the form of multi-hysteresis plots. Thus, on the one hand, the material behavior could be described in a one-dimensional stress state and, on the other hand, in a plane distortion state (Fig. 3). Four amplitudes were tested, each with five cycles (Fig. 4). The arithmetical mean value of the loading and unloading curve of the last cycle with maximum amplitude was chosen as the respective reference curve. It could be assumed that non-elastic effects were minimized with increasing cycle numbers and a quasi-static material state was established.

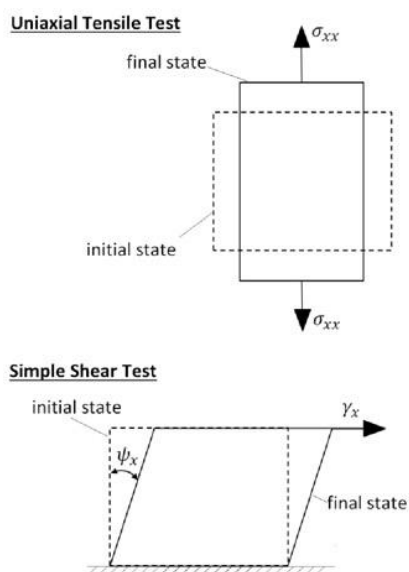


Fig. 3: Schematic diagram of the single-axis tensile test (top) and the simple shear test (bottom)

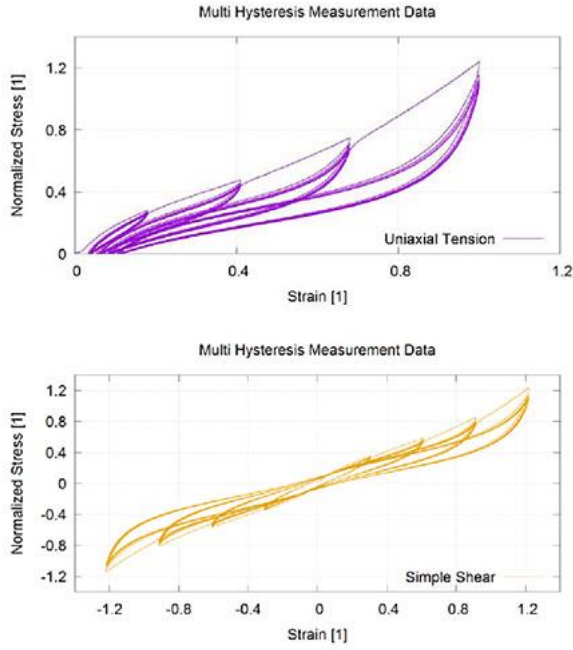


Fig. 4: Measurement data of the tensile test (top) and the simple shear test (bottom) [2]

This project focused on the determination of the material constants μ_i and α_i for the third-order Ogden model. This model describes the distortion energy \widehat{W} as a function of the spatial strains λ_i in the form of equation (1).

$$\widehat{W} = \sum_{i=1}^{\infty} \frac{\mu_i}{\alpha_i} (\lambda_1^{\alpha_i} + \lambda_2^{\alpha_i} + \lambda_3^{\alpha_i} - 3) \quad (1)$$

The assumption of the incompressibility according to equation (2) applies for the volume expansion J (see also [1]).

$$J = \lambda_1 \lambda_2 \lambda_3 = 1 \quad (2)$$

For loading and unloading, an average curve had to be found that passes through the origin point of the coordinate system. In the area of plastic expansion, the curve should have a slope as small as possible. Using one curve, the different material effects could thus be described in a corresponding manner (Fig. 5) because the third-order Ogden material model does not allow to consider inelastic effects directly, such as hysteresis loops and plastic strains.

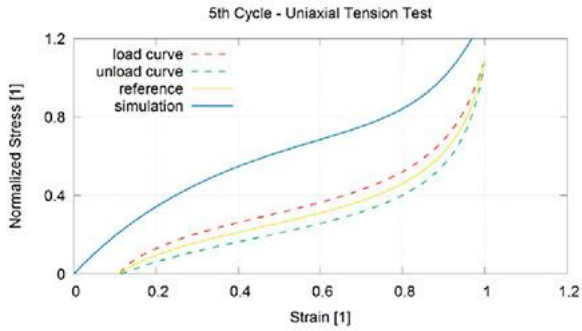


Fig. 5: Hysteresis of the normalized stress-strain curve for the tensile test

Parameter identification

The correlation between material parameters and the material behavior occurring during loading was determined inversely using the simulation of the material tests (Fig. 6).

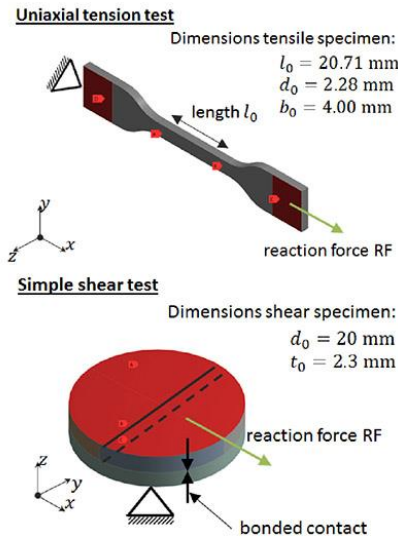


Fig. 6: Simulation models of the material tests for tensile test (top) and simple shear test (bottom)

Unfortunately, in ANSYS Workbench version 17.0, there is no option to use experimental test data from a tensile test and a simple shear test in the curve fitting simultaneously. The sensitivity study and the optimization (curve fitting) were carried out in optiSLang for parameter variation as well as for matching the reference curves with the simulation results.

Sensitivity analysis

The sensitivity study analyzes the influence of the individual parameters on the system behavior and limits their range of values for the subsequent curve fitting (Table 1).

i	α_i	μ_i	a_i	b_i
1	2 ... 4,5	0 ... 0,3	1	1
2	1	50 ... 100	-2 ... -1,5	1
3	16,5 ... 20,5	1	1	-6 ... -4

Table 1: Parameter range of the sensitivity study

In the parameter setting, the values α_2 and μ_3 were defined as dependent parameters according to (3.1) and (3.2). Thus, an equal distribution of parameter variation over more than one magnitude of the exponent was reached by using an Advanced Latin Hypercube Sampling. As a result, only the value ranges of the exponents were varied.

$$\alpha_i = 10^{a_i} \quad (3.1)$$

$$\mu_i = 10^{b_i} \quad (3.2)$$

For a robust physical material behavior, parameters with the same indices should have the same sign in accordance to condition (4). [1]

$$\alpha_i \mu_i > 0 \quad (4)$$

The equidistant discretized curves could be compared by using the Euclidean norm (*NRMS*) according to equation (5).

$$NRMS = \frac{\sqrt{\frac{1}{n} \sum_{i=1}^m (\sigma_{ref} - \sigma_{stm})^2}}{(\sigma_{max} - \sigma_{min})} \quad (5)$$

The prognosis capability of the simulation models proved to be very sufficient, which was indicated by a high Coefficient of Prognosis (CoP) for the overall model (see Fig. 7, red marking).

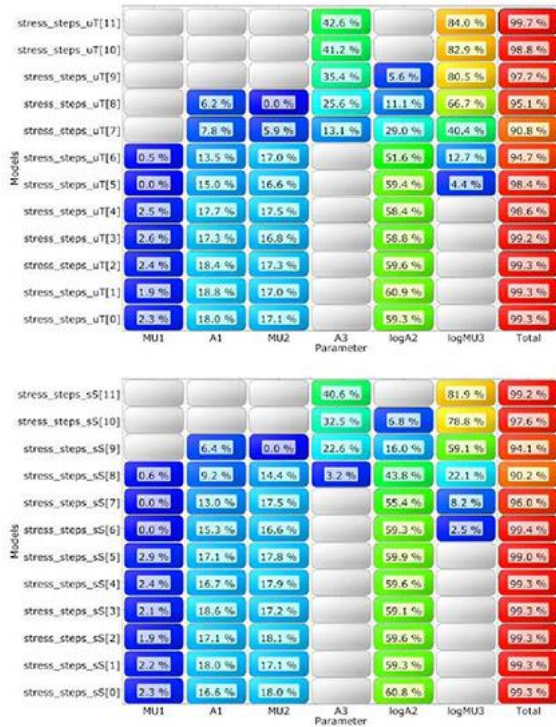


Fig. 7: CoP matrix of discretized signals for tensile test (top) and shear test (bottom)

A coupling of the significant parameters among each other was indicated by the sum of the single CoPs, which showed the influence of the input parameters. The parameters α_2 in the form of $logA2$ and α_1 , as well as μ_1 had a significant influence of up to 60 percent of the total strain. The remaining 40 percent showed an increasing influence of the parameter μ_3 , in the form of the exponents $logMU3$ and α_3 . For a subsequent optimization, the parameter range was considered to be sufficiently accurate since stress-strain curves of the calculated parameter variants covered the reference curves (Fig. 8).

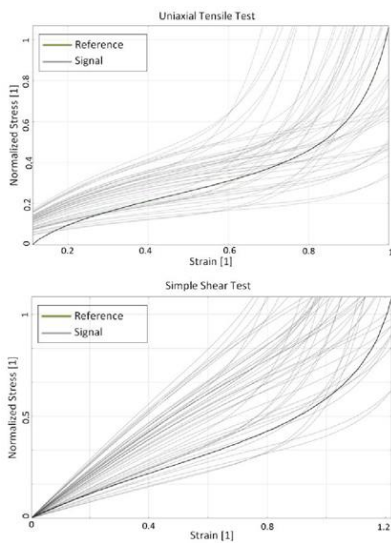


Fig. 8: Stress-strain curves for tensile test (top) and shear test (bottom)

Optimization

The fitting of the stress-strain curves from the material test simulations to the reference curves was defined as an optimization objective. The sum of the individual Euclidean norms per experiment defined the target function and had to be minimized according to equation (7). In contrast to simple shear tests, the measured values of the tensile test can be determined relatively easily with high accuracy and were therefore more weighted in the simulation.

$$\sum_{i=1}^n NRMS = \alpha \cdot NRMS_1 + \beta \cdot NRMS_2 \quad (7.1)$$

$$\sum_{i=1}^n NRMS \rightarrow 0 \quad (7.2)$$

The highly non-linear behavior of the Ogden material model required a direct optimization. Here, the ARSM algorithm (Adaptive Response Surface Method) was used. A comparison of the reference curves with the stress-strain curves of the best design parameter set showed a very accurate correspondence to the tensile test over the entire strain range (Fig. 9). A sufficient coverage of the curves up to a strain of 1 was achieved for the simple shear test.

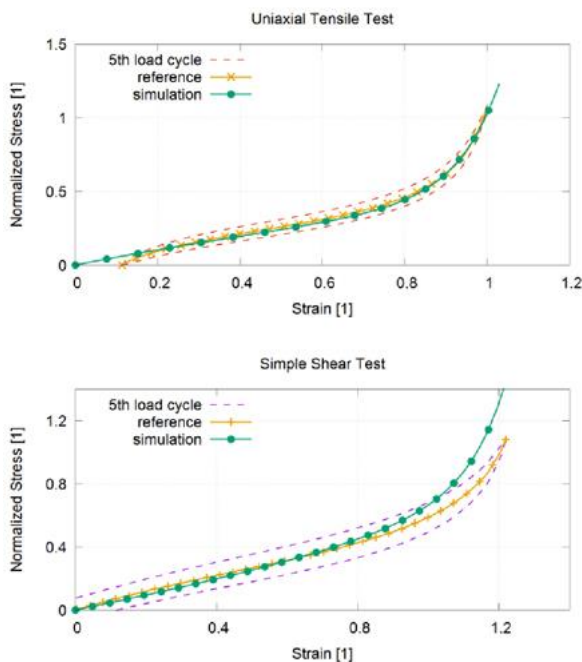


Fig.9: Comparison of the material test simulation with measurement data for tensile test (top) and shear test (bottom)

Axial-symmetrical 2D-simulation of an elastomer rubber boot

The third-order Ogden material model (Fig. 10) could then be used to analyze the component deformation. The aim was to obtain a reliable prognosis of potential contact points between the

boot and other joint components in order to eliminate damage to the boot surface in operational load cases.

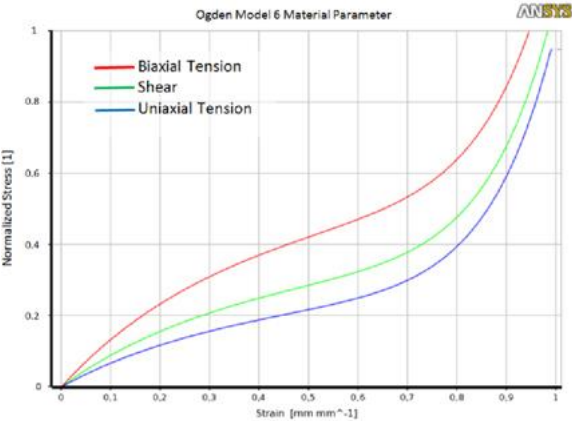


Fig. 10: Normalized stress-strain curves of the tensile (biaxial, uniaxial) and shear components

Furthermore, a fluid penetration test was carried out to determine whether the contact pressure on the shaft extension and in the sealing cap could ensure the leak tightness of the joint. For this purpose, a static, two-dimensional and axially symmetrical model of the CV joint was created. For simplification, the rolling elements were dispensed and contact situations between other joint components were replaced by boundary conditions. The non-deformed elastomeric boot (Fig. 11, top) first had to be placed in its installation position (Fig. 11, bottom). The subsequent application of negative length compensation and additional fluid pressure load showed that the boot fixation in the sealing cap and on the pin ensured the tightness of the joint (Fig. 12). Consequently, the sealing cap crimp and the clamp were sufficiently dimensioned to generate the required contact pressure. However, an increasing "s-punch shaped" deformation of the boot could be observed with increasing fluid pressure and length compensation. The deformation was eventually limited by the self-contact of the boot surface (Fig. 13 bottom).

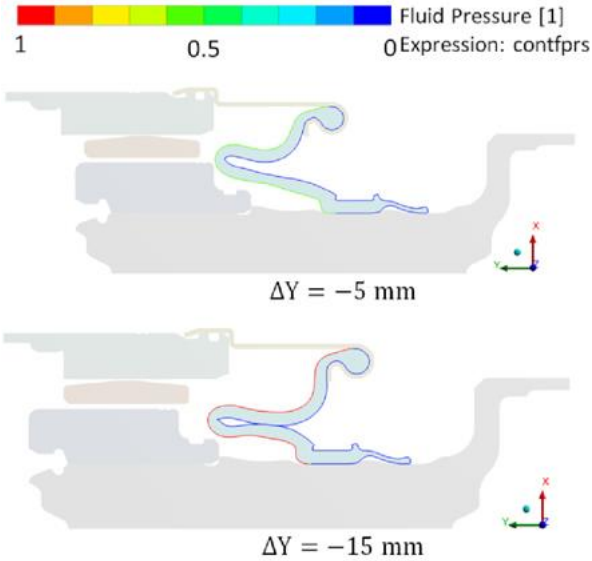


Fig. 11: Boot CAD part (top), 2D-axial-symmetrical model with built-in boot (bottom)

The maximum major strains (Hencky strains) reached a value of $\epsilon_{ux}^H = 0.52$. The relation between engineering strains and true strains is given by equation (8), according to [3]. With a strain $\epsilon = 0.68$, the deformations were within the area of the fitted curves showing a sufficient match with the measured values.

$$\epsilon_{ux}^H = \ln(\epsilon + 1) \quad (8)$$

To improve the convergence behavior, a non-linear stabilization method was used to control the dissipation of the element energy. [4] The simulation results of the boot deformations could be sufficiently compared with component deformations in pneumatic experiments, which were used for validation purposes. [2]

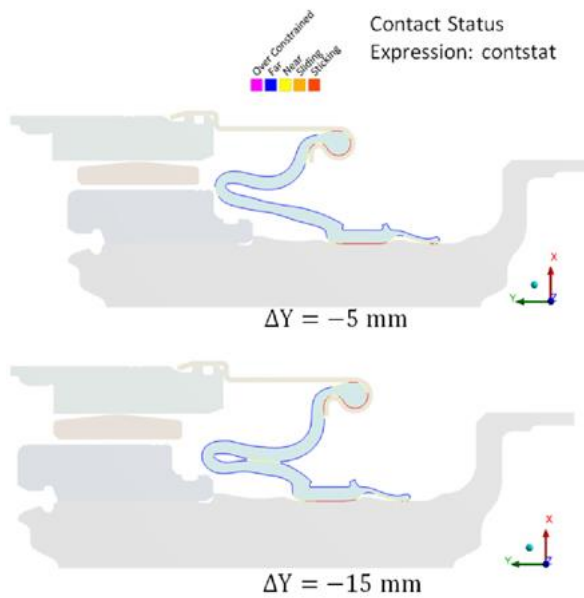


Fig. 12: Fluid pressure as a function of axial length compensation with distinctive s-punch shape (bottom)

Conclusion

The results of a fluid penetration analysis presented in this article were obtained by using a two dimensional axis symmetric model. The results showed an increased s-punch shaped deformation of the rubber boot caused by increasing a length change compensation of the CV joint and an additional fluid pressure load. Finally, the deformation stopped with self-contact at the boot surface. This result correlated well with pneumatic experiments.

Using optiSLang, tensile test data as well as simple shear test data for the third order Ogden material model could be taken into account. The found parameter set showed a very accurate match for tensile and simple shear test up to a stress of 1. The maximum major strains of this magnitude also corresponded to the analysis of the boot deformation in a two-dimensional, axially symmetrical model. The function and the deformations of the boot could be proven and reliably predicted using a fluid penetration analysis. In a next step following the simulation, the approach shall be transferred to a real three-dimensional joint geometry in order to examine the deformation behavior of the boot during gimbal joint movements.

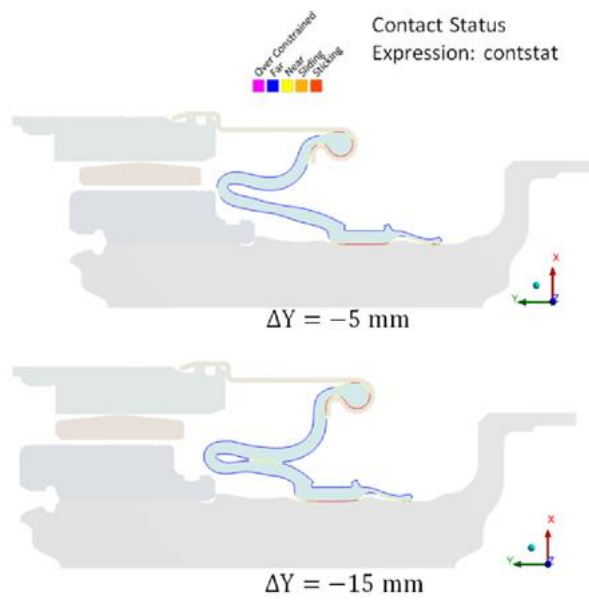


Fig. 13: Contact situation as a function of the axial length compensation and fluid pressure

Sources

- [1] R. W. Ogden, G. Saccomandi, I. Sagara: *Fitting hyperelastische models to experimental data*, Computational Mechanics, Springer-Verlag, 2004
- [2] IFA: *Interner Prüfbericht*, 2015
- [3] H. Mang, G. Hofstetter: *Festigkeitslehre*, Springer Verlag, 2000 ISBN: 978-3-7091,3762-8
- [4] R. Cisloiu, J. Wang: *Understanding Nonlinear Stabilization Features*, ANSYS Solutions Magazine Volume 7, Issue , 2006